GPPS | JOURNAL

JOURNAL OF THE GLOBAL POWER AND PROPULSION SOCIETY
journal.gpps.global

Systematic Roughness Variation to Model the Influence of Skewness on Wall Bounded Flows

Original article

Article history:
Submission date: 18 October 2022
Acceptance date: 5 April 2023
Publication date: 14 June 2023

This is the updated version of a paper originally presented at the Global Power and Propulsion Technical Conference, GPPS Chania22, September 11–14, 2022.

***Correspondence:**
SK: kurth@tfd.uni-hannover.de
KC: cengiz@tfd.uni-hannover.de

Peer review:
Single blind

Keywords:
roughness; skewness; wall bounded flows; modeling; DNS

Citation:
Kurth S., Cengiz K., Möller D., Wein L., and Seume J. R. (2023). Systematic Roughness Variation to Model the Influence of Skewness on Wall Bounded Flows. Journal of the Global Power and Propulsion Society. 7: 177–187.
https://doi.org/10.33737/jgpps/163089

Sebastian Kurth[1,*], Kenan Cengiz[1,*], Daniel Möller[2], Lars Wein[1], Joerg R. Seume[1]

[1]*Leibniz Universität Hannover, Institute of Turbomachinery and Fluid Dynamics, An der Universität 1, 30823 Garbsen, Hannover, Germany*
[2]*MTU Aero Engines AG, Dachauer Str. 665, 80995 Munich, Germany*

Abstract

In recent years, the research on roughness has focused on various roughness features, rather than the roughness height only, in order to improve the understanding of roughness effects on wall bounded flows. A special focus is placed on the skewness of the roughness height profile. The skewness measures whether the height profile is dominated by negative or positive roughness elements. Surfaces with both features can be found on worn blades: On the leading edge, roughness is caused by the impact of particles resulting in a negative skewness. Rough surfaces around the trailing edge, however, develop due to depositions leading to a positive skewness.

In this paper, rough surfaces taken from a compressor blade of an aero engine are systematically varied to investigate the isolated effect of skewness on aerodynamic losses. By direct numerical simulations of a periodic flow channel. The results show that the skewness has a major influence on loss generation. Based on these results, an existing model which essentially uses the shape-and-density parameter, is extended by a skewness factor. The modified correlation predicts the influence of the rough surfaces investigated well.

Introduction

Rough surfaces influence the aerodynamics of turbomachinery, e.g. aero engines. In general, roughness increases losses in the flow due to higher production of turbulence: higher turbulence due to a change in momentum transfer between fluid and surface leads to higher losses. The increase of losses also leads to a decrease of the fluid's velocity close to the wall and thereby an increase of the boundary layer thickness. Also other properties of the blade like the location of separation bubbles or the transition point are affected by the change of the boundary layer flow (Roberts and Yaras, 2005).

The velocity defect induced by the roughness leads to a deflection of the wake, and a change of incidence angle on the stage downstream. A disturbance of the incidence, for example in a compressor, can reduce the performance by up to 2.5% (Seehausen et al., 2020). Examples for the diverse types of roughness, found on worn blades of an airplane engine, are shown in Figure 1. The roughness depends on the location of the blade in the engine and on the position on the blade (Gilge et al., 2019a). In low-fidelity simulations like RANS, the boundary condition is modified to take the roughness of the wall into account. In the $k-\omega$ turbulence model by Wilcox (1988) for instance, the roughness is described by a single parameter, the equivalent sand grain roughness ks,

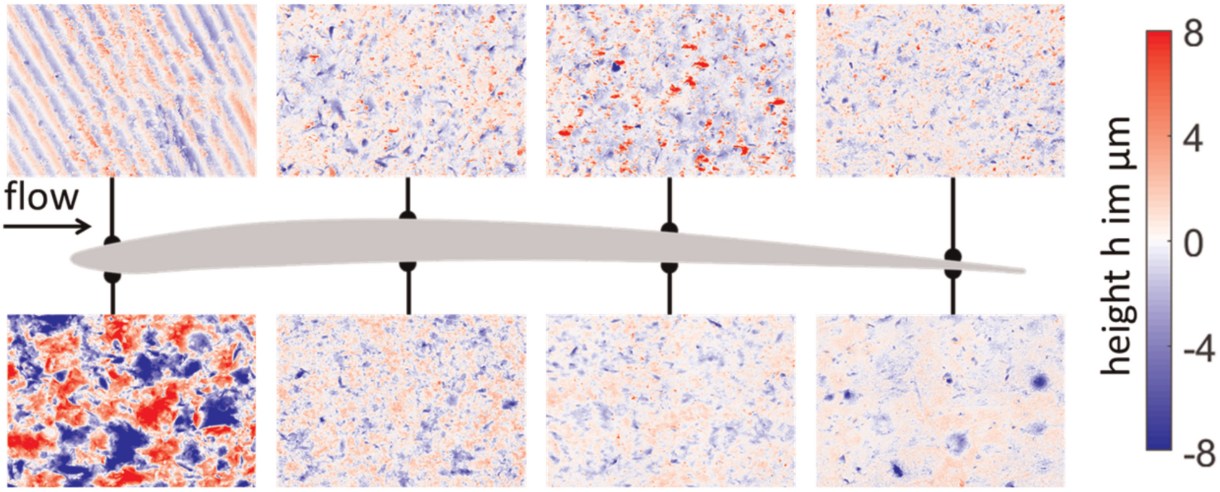

Figure 1. Examples of roughness measured on the blades of the third stage of a compressor adopted from (Gilge et al., 2019a). An extended collection of roughness measurements from worn compressor blades and a worn blisk can be found in (Gilge et al., 2019b).

to modify the ω boundary condition. The equivalent sand grain roughness is correlated with the roughness topology. Bons (2010) gives an overview about the many existing approaches to correlate ks with the profile of the rough surface. These correlations either use parameters calculated from linear surface height measurements ($h = f(x)$) or areal surface measurements ($h = f(x, y)$), as defined in various industrial standards (DIN EN ISO 4287, 2009; DIN EN ISO 25178-2, 2012).

To develop new models, or to improve the existing turbulence models and the ks correlations, results from experiments or direct numerical simulations (DNS) can be used. In recent years, an increased focus is set on the influence of the skewness parameter SSk, the effective slope ES or the arithmetic roughness height Sa. Experimental studies by Flack et al. (2020) and numerical simulations by Kuwata and Nagura (2020) show, that positively-skewed surfaces have a higher influence on the flow than negatively-skewed surfaces. The roughness peaks of positively-skewed surfaces reach further into the boundary layer and increase the drag and the turbulence production (Jelly and Busse, 2018). Flack et al. (2020) also show that the drag created by rough surfaces, is more sensitive to the root mean square roughness height when the surface is positively-skewed than negatively-skewed. Kuwata and Nagura (2020) show that the drag is equally sensitivity to the effective slope of the roughness elements. The effective slope ES is changed from ES = 0.1 to ES = 0.6 by compressing the roughness in the horizontal dimensions. The influence of the effective slope on the flow, measured by an decrease of the roughness function ΔU^+, is not linear. For ES < 0.4 a steady decrease of ΔU^+ can be observed, getting smaller for ES > 0.4. An explanation for this effect can be found when analyzing the composition of the total flow resistance, which consists of the viscous drag and the pressure drag. With an increasing effective slope, the ratio of pressure drag to viscous drag is increasing and becomes dominant for ES > 0.4. Comparable observations are also made by Ahrens et al. (2021), who investigate the influence of the relative angle between the flow and the dominant direction of anisotropic rough surfaces. By changing the flow angle, the observed effective slope by the flow is changed and thereby the ratio of pressure to viscous drag.

This brief (and by far not full overview) of recent research shows the many influencing factors that need to be considered for modeling the influence of roughness on wall bounded flows. In this paper, further investigations into the influence of roughness skewness are conducted, with the aim to find a new or to improve an existing ks-correlation for rough surfaces found on aero engine blades. To investigate the influence of single roughness parameters independently, direct numerical simulations of systematically varied rough surfaces are conducted.

Systematically varied real roughness

Two roughness, found on compressor blades of a medium size high-bypass aircraft engine, are used as a basis for this investigation (Gilge et al., 2019b). An overview is shown in Figure 2. A confocal microscope is used to measure the surfaces height on equidistant scanning points ($\Delta x^+ = \Delta y^+ = 1.5$). More information about the measurement and processing of the surfaces can be found in Gilge et al. (2019a) and Kurth et al. (2021). All

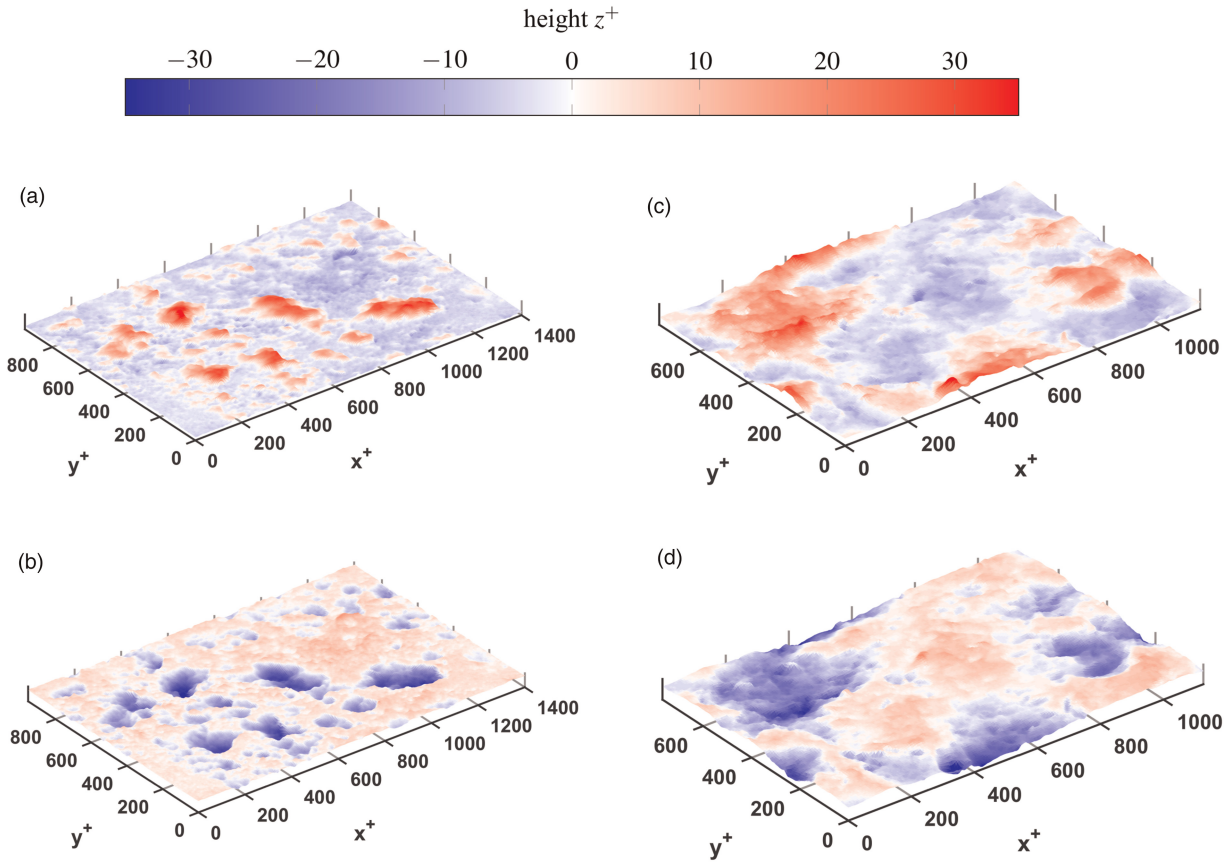

Figure 2. Base and mirrored roughnesses used for systematic variation of roughness density, height and skweness. Scaled for DNS with $\mathrm{Re}_\tau = 395$. (a) Reference Surface A (b) Mirrored Surface A (c) Mirrored Surface B (d) Reference Surface B.

physical distances s are non-dimensionalised by

$$s^+ = \frac{s \cdot u_\tau}{\nu} \tag{1}$$

with u_τ being the friction velocity, and ν being the kinematic viscosity of a smooth surface under the DNS flow conditions. Both reference surfaces are found on a blade from the third stage of a high-pressure compressor. reference surface A (Figure 2a) is found on the suction side and is dominated by deposits. reference surface B (Figure 2d) is found on the pressure side and was formed primarily by impacts. Both types of roughness are varied systematically to investigate the isolated influence of roughness skewness, height, and density. An overview for some parameters for all investigated surfaces is given in Table 1 in the appendix.

Isolation of roughness skewness

The skewness (SSk) of the roughness is a parameter used to quantify, whether a roughness consists primarily of hills (SSk $>$ 0; reference surface A) or valleys (SSk $<$ 0; reference surface B). By mirroring the reference surface on the x-y-plane, the skewness is inverted. This has the great advantage that all other parameters change little to none.

Variation of roughness height

To change the roughness height without changing it's density, all dimensions are multiplied by a scaling factor sf. For this paper, the base and the mirrored roughness were varied with scaling factors of sf $= 0.8$ and 1.2 respectively. The change of roughness height is influencing roughness parameters like the mean roughness height Sa or the equivalent sand-grain roughness ks. Other parameters like the skewness SSk of the roughness or the effective slope Es are not changed.

Table 1. Roughness parameters of simulated surfaces.

	Base Roughness	Mirrored	Scaling Factor										
			sf_x	sf_y	sf_z	Sa^+	Sz^+	SSk	SKu	Esx	ks^+_{Sa}	ks^+_{SD}	ks^+_{SDS}
Reference	A		1	1	1	5	29.6	1.9	7	0.19	26	23	23.6
	A	x	1	1	1	5	29.6	–1.9	7	0.19	26	24	8.6
	B		1	1	1	6.5	31.3	0.96	3.5	0.15	33.8	21	15
	B	x	1	1	1	6.5	31.3	–0.96	3.5	0.15	33.8	19.8	7.4
Roughness Height	A		0.8	0.8	0.8	4.1	23.7	1.9	7	0.19	21.3	18.5	18.9
	A	x	0.8	0.8	0.8	4.1	23.7	–1.9	7	0.19	21.3	19.4	6.9
	B		0.8	0.8	0.8	5.2	25	0.96	3.5	0.15	27	16.8	12
	B	x	0.8	0.8	0.8	5.2	25	–0.96	3.5	0.15	27	15.8	5.9
	A		1.2	1.2	1.2	6.1	35.5	1.9	7	0.19	31.7	27.7	28.4
	A	x	1.2	1.2	1.2	6.1	35.5	–1.9	7	0.19	31.7	29.1	10.4
	B		1.2	1.2	1.2	7.8	37.6	0.96	3.5	0.15	40.6	25.3	18
	B	x	1.2	1.2	1.2	7.8	37.6	–0.96	3.5	0.15	40.6	16.8	8.8
Roughness Density	A		0.8	0.8	1	5	29.6	1.9	7	0.23	26	29.3	30
	A	x	0.8	0.8	1	5	29.6	–1.9	7	0.23	26	30.7	11
	B		0.8	0.8	1	6.5	31.3	0.96	3.5	0.18	33.8	26.8	19.1
	B	x	0.8	0.8	1	6.5	31.3	–0.96	3.5	0.18	33.8	25.2	9.37
	A		1.2	1.2	1	5	29.6	1.9	7	0.17	26	18.9	19.4
	A	x	1.2	1.2	1	5	29.6	–1.9	7	0.17	26	20	7.1
	B		1.2	1.2	1	6.5	31.3	0.96	3.5	0.12	33.8	17.3	12.3
	B	x	1.2	1.2	1	6.5	31.3	–0.96	3.5	0.12	33.8	25.2	9.4

Variation of roughness density

By multiplying only the horizontal roughness dimensions (x and y) by a scaling factor sf, the density of the roughness is changed. Again, the base and mirrored roughness were varied with scaling factors of sf = 0.8 and 1.2 respectively. Because the roughness height does not change, parameters like the mean roughness height Sa and skewness SSk do not change. The equivalent sand-grain roughness height ks only changes, if it is based on the shape and density parameter but not, if it based on the mean roughness height Sa.

Numerical setup

In this study, an immersed boundary method (IBM) is adopted for direct numerical simulation (DNS) of the flow over the rough surface. This method has some advantages over the conventional body-fitted approach. Firstly, the mesh is regular with perfect quality, being independent of the immersed body. Secondly, the mesh

can also be used for other surfaces, simply because the introduction of the surface involves nothing but immersion in the computational domain. Last but not the least; the generation of the mesh requires very little human effort. The IBM approach used in this paper is provided in *foam-extend-4.0*. It is based on the polynomial fitting of the solution on the IB cells concerning the boundary condition on the wall. A detailed explanation of the method can be found in Senturk et al. (2019).

The CFD tool used, *foam-extend-4.0*, is based on a cell-centered finite volume discretization. For the incompressible solver based on *icoFoam*, Gauss linear scheme and backward temporal discretization are chosen, resulting in second-order accuracy both in time and space. PISO algorithm is used for the solution of the incompressible flow equations. For all the simulations, a maximum CFL number smaller than 0.5 is ensured.

A channel setup is convenient to investigate the flow over a roughness patch because the friction velocity Reynolds number

$$\mathrm{Re}_\tau = \frac{u_\tau \cdot \delta}{\nu} \tag{2}$$

can easily be set through the incorporation of a constant body force in the momentum equations. Hence, the drag on the surface is balanced by this flow-driving force as long as the flow is fully developed. The boundary layer thickness δ is fixed by half channel height, where symmetric conditions are imposed. Moreover, periodicity is imposed on the lateral boundaries to enable not only the use of a smaller domain but also the use of spatial averaging for better flow statistics. On the bottom wall, the roughness patch is immersed in the mesh ensuring no-slip condition. The mean height of the surface corresponds to the $z = 0$ plane (Figure 3). The periodicity of the roughness patch is ensured by using a linear blending function to blend 10% of the roughness patch on the borders. The structured computational mesh is generated using constant spacing in both of the lateral directions.

The mesh consists of $n_X \times n_y \times n_z = 200 \times 138 \times 160 \approx 4.4 \cdot 10^6$ cells, resulting in a lateral mesh spacing of $\Delta x^+ = \Delta y^+ = 7.3$. The mesh resolution study included in Kurth et al. (2021) shows, that this resolution still allows for accurate DNS results. In the wall-normal direction, the channel is split into three blocks: the IB block with a constant spacing $z^+ \approx 0.9$, the transition block with a growth rate of less than 6%, and the core block with a constant spacing of $z^+ \approx 4.9$. In this study, a friction Reynolds number of $\mathrm{Re}_\tau \approx 395$ is enforced for all of the simulations. As soon as the flow is developed, statistics are collected for a sufficient amount of convection time. The statistics are then averaged both spatially and temporally. Figure 4 shows the three momentary velocity components at a time step for the vertical mid-plane of the computational domain, as an example for the simulation results. The roughness can be recognized at the bottom of the surface plot. It is influencing the flow by deflecting the flow in vertical and horizontal direction.

The DNS-IBM approach is validated with the $Re_\tau \approx 180$ channel setup on a smooth surface with the highly resolved DNS results, as well as on a rough surface. All the validation results can be found in the previous communication Kurth et al. (2021).

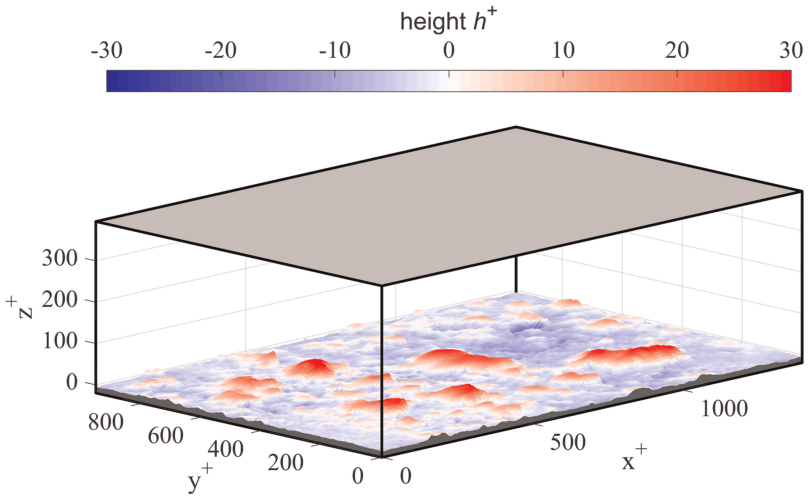

Figure 3. Double-infinite channel with rough surfaces on bottom wall. The channel is symmetric in wall-normal direction with the gray plane being the symmetry plane.

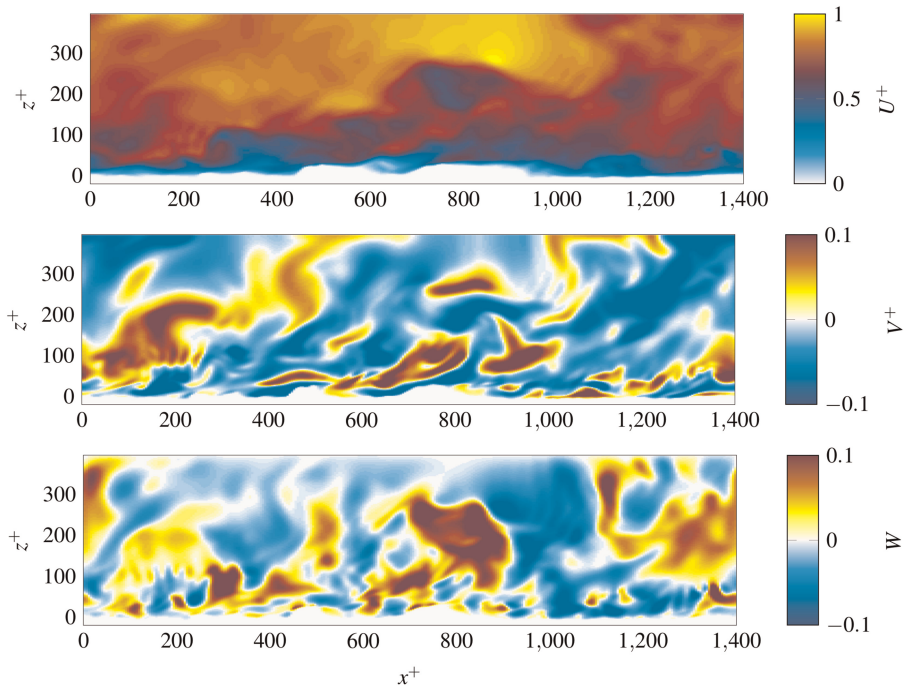

Figure 4. Excerpt of DNS simulation of Reference Surface A. The three momentary velocity components at the vertical mid-plane of the computational domain are shown.

Results

During the simulation, the friction velocity Reynolds number (Equation 2) is kept constant by applying a constant body force on the fluid. An increase of losses by the roughness is therefore shown as a decrease of the mass flow. In the velocity profiles, shown in Figure 5, this decrease of mass flow is reflected by a decrease of velocity. In comparison with the results of a smooth channel DNS, the simulations with a roughness show a velocity deficit ΔU^+. Despite keeping roughness parameters other than the skewness constant, both types of roughness show considerably different velocity deficits. This confirms the importance of roughness skewness for building or improving a ks-correlation.

Figure 6 shows the velocity deficit ΔU^+ and the ks^+ value, calculated with two different correlations, for each investigated surface. The correlation by Hummel et al. (2004)

$$\mathrm{ks}_{\mathrm{Sa}} = 5.2 \cdot \mathrm{Sa} \tag{3}$$

uses the mean roughness height

$$\mathrm{Sa} = \iint_A h \; dx\,dy \tag{4}$$

The correlations by Bons (2005)

$$\frac{\mathrm{ks}_{\mathrm{SD}}}{k} = 0.43 \cdot \log\left(\Lambda_S\right) + 0.82 \tag{5}$$

use the shape and density parameter

$$\Lambda_S = \frac{S}{S_f}\left(\frac{A_f}{A_s}\right)^{-1.6}, \tag{6}$$

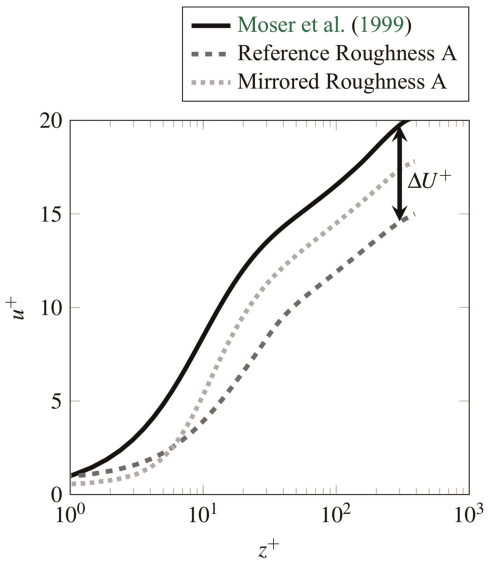

Figure 5. Boundary layer profile of Reference Roughness A and Mirrored Roughness A compared to smooth channel DNS results by Moser et al. (1999). The velocity defect ΔU^+ is defined as difference between the velocity profiles in the log-law region.

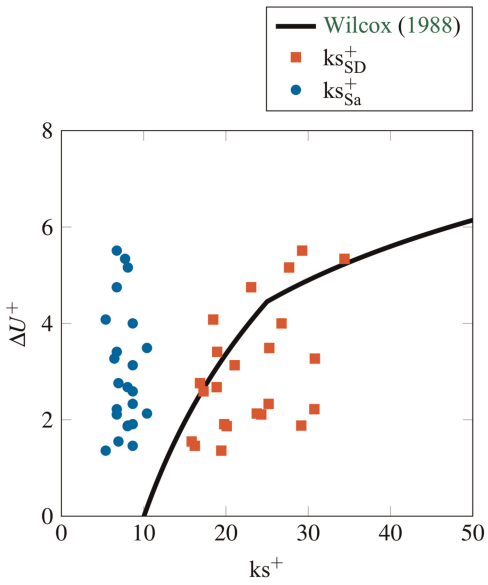

Figure 6. Comparison of ks^+ values calculated with the correlation by Hummel et al. (2004) (ks^+_{Sa}) and Bons (2005) (ks^+_{SD}) to the velocity defect calculated from the DNS results.

by Dirling (1973). The shape and density parameter evaluates the density of the roughness elements and the gradient (shape) of the roughness elements. For the roughness height k the maximum roughness height Sz is used. Both correlations can't predict the equivalent sand grain roughness ks correctly. The ks^+ values calculated with the correlation by Hummel et al. (2004) have less variation, because it is only based on the mean roughness height Sa. The ks^+ values calculated with the correlation by Bons (2005) span a broader region. However, both correlations fail, as very similar ks^+ values are calculated despite the significantly different velocity deficits ΔU^+.

Within the $k-\omega-$ turbulence model by Wilcox (1988), the wall function is defined by

$$U^+ = \frac{1}{\kappa}\ln y^+ + B \tag{7}$$

The constant B depends on the roughness of the wall. For smooth surfaces it is given as

$$B = \lim_{y^+\to\infty}\left[U^+ - \frac{1}{\kappa}\ln y^+\right] = 5.1 \tag{8}$$

For rough surfaces it is given as

$$B = 8.4 + \frac{1}{\kappa}\ln\frac{S_R}{100} \tag{9}$$

with

$$S_R = \begin{cases} \left(\dfrac{50}{ks^+}\right)^2, & ks^+ < 25 \\ \dfrac{100}{ks^+}, & ks^+ \geq 25 \end{cases} \tag{10}$$

The velocity difference for a given equivalent surface roughness ks^+ can be calculated by the difference of the smooth (U_S^+) and rough (U_R^+) wall function:

$$\Delta U^+ = U_S^+ - U_R^+ = f(\mathrm{ks}^+) = \begin{cases} \frac{1}{\kappa}\ln\left(\frac{(\mathrm{ks}^+)^2}{25}\right) - 3.4, & \mathrm{ks}^+ < 25 \\ \frac{1}{\kappa}\ln(\mathrm{ks}^+) - 3.4, & \mathrm{ks}^+ \geq 25 \end{cases} \tag{11}$$

The accuracy of a ks-correlation can be evaluated by the fit of its prediction of ks^+ to Equation 11. The coefficient of determination is $R^2 = 0.02$ for the correlation by Hummel et al. (2004) and $R^2 = 0.11$ for the correlation by Bons (2005).

Modelling the influence of skewness

A correlation matrix is used to identify or improve correlations from the roughness geometry to the DNS results. Figure 7 shows an excerpt of a correlation matrix for the given DNS results. Roughness parameters, calculated from the roughness geometry, are listed on the abscissa. On the ordinate, values deduced from the DNS are listed. Solving Equation 11 for the equivalent sand grain roughness ks^+ results in a function to calculate the sand-grain roughness $\mathrm{ks}_{\Delta U^+}$, that must be set as roughness in the low order simulation to achieve the same velocity deficit ΔU^+ as observed in DNS:

$$\mathrm{ks}^+_{\Delta U^+} = f(\Delta U^+) = \begin{cases} 5 \cdot \sqrt{e^{\kappa\cdot(\Delta U^+ + 3.4)}}, & \Delta U^+ < 4.6472 \\ e^{\kappa\cdot(\Delta U^+ + 3.4)}, & \Delta U^+ \geq 4.6472 \end{cases} \tag{12}$$

The coefficient of determination R^2 of the *2nd* order polynomial correlation fit is color coded: the darker the color, the better the fit. It can be seen, that no roughness parameter except of the skewness shows a good fit to the observed DNS results. The best correlation ($R^2 \approx 0.93$) is found for the skewness to the ratio of $\mathrm{ks}^+_{\mathrm{SD}}$ to $\mathrm{ks}^+_{\Delta U^+}$. Figure 8 shows the correlation function

$$\epsilon_{\mathrm{ks,SD}} = \frac{\mathrm{ks}^+_{\mathrm{SD}}}{\mathrm{ks}^+_{\Delta U^+}} = f(SSk) = 0.02664 \cdot \mathrm{SSk}^2 + 0.1426 \cdot \mathrm{SSk} + 0.7977 \tag{13}$$

Most DNS results are within the 95% functional confidence interval shown as a gray shadow. Based on the found correlation, the ks-correlation based on the shape and density parameter can be improved.

The equivalent sand grain roughness

$$\frac{\mathrm{ks}_{\mathrm{SD}}}{k} = \epsilon_{\mathrm{ks,SD}} \cdot (0.43 \cdot \log(\Lambda_S) + 0.82) \tag{14}$$

calculated from the roughness geometry with the correlation based on the shape, density and skewness parameter is shown in Figure 9. The factor $\epsilon_{\mathrm{ks,SD}}$ can be seen as a scaling factor, depending on the skewness of the

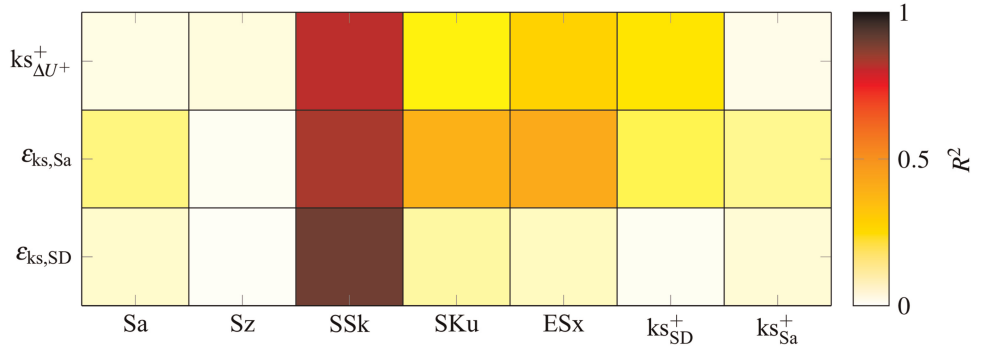

Figure 7. Excerpt of correlation map for roughness parameters and DNS results.

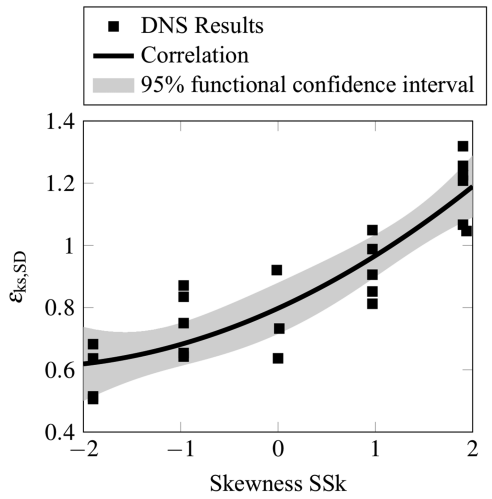

Figure 8. Correlation function for skewness to relative ratio of the ks-correlation based on shape and density parameter and the ks-value based on velocity deficit ΔU^+ from DNS results.

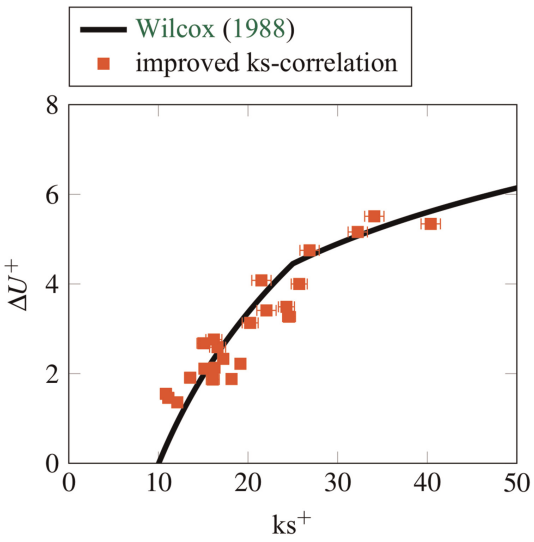

Figure 9. New ks-correlation based on Shape-, Density- & Skewness-Parameter.

roughness. For large positive skewness, the scaling factor is close to 1. The ks-value is about the same as calculated with the shape and density parameter. For smaller and negative skewed roughness profiles, the $\epsilon_{ks,SD}$ is < 1. The equivalent sand grain roughness calculated with the shape an density parameter is decreased. A great improvement in predicting the influence of the investigated roughness is achieved. The coefficient of determination for the improved correlation is $R^2 = 0.90$, compared to $R^2 = 0.11$ for the correlation by Sigal and Danberg (1990). The equivalent sand grain roughness of all surfaces can be calculated to predict the correct influence on the flow even with RANS.

Conclusions

The aim of this investigation is to improve the equivalent sand grain roughness (ks) correlation for surfaces from aero engines. To achieve this, direct numerical simulations (DNS) of channel flows with systematically varied rough surfaces are carried out at a friction Reynolds number of $\mathrm{Re}_\tau = 395$. Two rough surfaces are taken from the compressor blades of a medium size high bypass aircraft engine. They are varied by stretching and compressing to change the roughness density and height. Additionally, all rough surfaces are mirrored on the horizontal plane to change their skewness without changing any other parameters. The mirrored surfaces are found to have a significantly different effect on the flow, even though the same equivalent sand grain roughness is calculated by existing correlations. The DNS results are correlated with various roughness parameters. The best results are achieved when correlating the skewness of the roughness with the quotient of the ks value based on the shape and density parameter and the ks value based on the velocity deficit from the DNS. Extending the correlation based on the shape and density parameter, with a function based on the skewness parameter, the ks-correlation is improved from $R^2 = 0.11$ to $R^2 = 0.90$. The improved ks-correlation needs to be validated in future investigations.

Nomenclature

ESi	effective slope in x-direction	$(A^{-1} \iint_A \frac{\partial h}{\partial i} \mathrm{d}A)$
ks	equivalent sand grain roughness	(equ. 12, 3, 5)
ks^+	normalized equivalent sand grain roughness	$(u_\tau \cdot \mathrm{ks} \cdot \nu^{-1})$
n_x, n_y, n_z	number of cells	$(-)$
Re_τ	shear stress Reynolds number	$(u_\tau \cdot \delta \cdot \nu^{-1})$
R^2	coefficient of determination	$(-)$
Sa	mean roughness height	$(A^{-1} \iint_A \lvert h \rvert \mathrm{d}A)$

sf	scaling factor	(–)
SKu	kurtosis of height values	$(Sq^{-4}A^{-1}\iint_A h^3 \mathrm{d}A)$
SSk	sknewess of height values	$(Sq^{-3}A^{-1}\iint_A h^3 \mathrm{d}A)$
Sq	root mean square roughness height	$(\sqrt{A^{-1}\iint_A z_h^2(x)\mathrm{d}A})$
Sz	maximum roughness height	(–)
u_τ	friction velocity	$(\sqrt{\tau_\mathrm{W}\cdot\rho^{-1}})$
u, v, w	Velocities	(–)
u^+, v^+, w^+	normalized velocities	$(u\cdot u_\tau^{-1})$
x, y, z	spatial coordinates	(–)
x^+, y^+, z^+	normalized spatial coordinates	$(u_\tau\cdot \mathrm{x}\cdot\nu^{-1})$
δ	channel half height	(–)
$\epsilon_{\mathrm{ks,i}}$	correlation function	$(\mathrm{ks}^+_{\mathrm{SD}}/\mathrm{ks}^+_{\Delta U^+})$
U^+	roughness function	(–)
Λ_s	shape and density parameter	(–)
ν	kinematic viscosity	(–)
ρ	Density	(–)
τ_w	wall shear stress	(–)

Acknowledgments

The authors would like to thank the BMWi and DFG for the support. The authors would also like to thank the North-German Supercomputing Alliance (HLRN) for the HPC resources that have contributed to the development of the research results presented here.

Funding sources

Federal Ministry for Economic Affairs and Energy (BMWi) within their aviation research program (LuFo) under the funding code 20T1719C Deutsche Forschungsgemeinschaft (DFG, German Research Foundation) within the Collaborative Research Center (CRC) 871 “Regeneration of Complex Capital Goods.

Competing interests

Sebastian Kurth declares that he has no conflict of interest. Kenan Cengiz declares that he has no conflict of interest. Daniel Moeller declares that he has no conflict of interest. Lars Wein declares that he has no conflict of interest. Joerg R. Seume declares that he has no conflict of interest.

References

Ahrens J., Kurth S., Cengiz K., Wein L., and Seume J. (2021). Immersed boundary method for the investigation of real surfaces with isotropic and anisotropic roughness components. In Proceedings of the Global Power and Propulsion Society, Virtual Conference, Xi’an, China.

Bons J. (2005). A critical assessment of reynolds analogy for turbine flows. *Journal of Heat Transfer*. 127 (5): 472–485. https://doi.org/10.1115/1.1861919.

Bons J. P. (2010). A review of surface roughness effects in gas turbines. *Journal of Turbomachinery*. 132 (2): 021004. https://doi.org/10.1115/1.3066315.

DIN EN ISO 25178-2. (2012). Geometrische Produktspezifikation (GPS) – Oberflächen-beschaffenheit: Flächenhaft – Teil 2: Begriffe und Oberflächen-Kenngrößen (ISO 25178-2:2012), Deutsche Fassung EN ISO 25178-2:2012, *Beuth Verlag*.

DIN EN ISO 4287. (2009). Geometrische Produktspezifikation (GPS) – Oberflächen-beschaffenheit: Tastschnittverfahren - Benennungen, Definitionen und Kenngrößen der Oberflächenbeschaffenheit (ISO 4287:1997 + Cor 1:1998 + Cor 2:2005 + Amd 1:2009), Deutsche Fassung EN ISO 4287:1998 + AC:2008 + A1:2009, *Beuth Verlag*.

Dirling R. (1973). A method for computing roughwall heat transfer rates on reentry nosetips. In 8th Thermophysics Conference, p. 763.

Flack K., Schultz M., and Barros J. (2020). Skin friction measurements of systematically-varied roughness: probing the role of roughness amplitude and skewness. *Flow, Turbulence and Combustion*. 104 (2): 317–329. https://doi.org/10.1007/s10494-019-00077-1.

Gilge P., Kellersmann A., Friedrichs J., and Seume J. R. (2019a). Surface roughness of real operationally used compressor blade and blisk. *Proceedings of the Institution of Mechanical Engineers, Part G: Journal of Aerospace Engineering*. 233 (14): 5321–5330. https://doi.org/10.1177/0954410019843438.

Gilge P., Kellersmann A., Kurth S., Friedrichs J., and Seume J. R. (2019b). Dataset: Surface roughness of real operationally used compressor blade and blisk. https://doi.org/10.25835/0084372.

Hummel F., Lötzerich M., Cardamone P., and Fottner L. (2004). Surface roughness effects on turbine blade aerodynamics. *Journal of Turbomachinery*. 127 (3): 453–461. https://doi.org/10.1115/1.1860377.

Jelly T. O. and Busse A. (2018). Reynolds and dispersive shear stress contributions above highly skewed roughness. *Journal of Fluid Mechanics*. 852: 710–724. https://doi.org/10.1017/jfm.2018.541.

Kurth S., Cengiz K., Wein L., and Seume J. (2021). From measurement to simulation - a review of aerodynamic investigations of real rough surfaces by dns. In Proceedings of the Global Power and Propulsion Society, Virtual Conference, Xi'an, China.

Kuwata Y. and Nagura R. (2020). Direct numerical simulation on the effects of surface slope and skewness on rough-wall turbulence. *Physics of Fluids*. 32 (10): 105113. https://doi.org/10.1063/5.0024038.

Moser R. D., Kim J., and Mansour N. N. (1999). Direct numerical simulation of turbulent channel flow up to re_τ=590. *Physics of fluids*. 11 (4): 943–945. https://doi.org/10.1063/1.869966.

Roberts S. K. and Yaras M. I. (2005). Effects of surface-roughness geometry on separation-bubble transition. *Journal of Turbomachinery*. 128 (2): 349–356. https://doi.org/10.1115/1.2101852.

Seehausen H., Gilge P., Kellersmann A., Friedrichs J., and Herbst F. (2020). Numerical study of stage roughness variations in a high pressure compressor. *International Journal of Gas Turbine, Propulsion and Power Systems*. 11 (3): 16–25. https://doi.org/10.38036/jgpp.11.3_16.

Senturk U., Brunner D., Jasak H., Herzog N., Rowley C. W., and Smits A. J. (2019). Benchmark simulations of flow past rigid bodies using an open-source, sharp interface immersed boundary method. *Progress in Computational Fluid Dynamics, an International Journal*. 19 (4): 205–219.

Sigal A. and Danberg J. E. (1990). New correlation of roughness density effect on the turbulent boundary layer. *AIAA Journal*. 28 (3): 554–556. https://doi.org/10.2514/3.10427.

Wilcox D. C. (1988). Reassessment of the scale-determining equation for advanced turbulence models. *AIAA Iournal*. 26 (11): 1299–1310. https://doi.org/10.2514/3.10041.